Evolution of Au $L\beta_2$ visible satellites around thresholds

H. Oohashi* and Y. Ito
Laboratory of Atomic & Molecular Physics, Institute for Chemical Research, Kyoto University, Gokasho, Uji, Kyoto 611-0011, Japan

T. Tochio
Keihanna Interaction Plaza Inc., Seika-cho Soraku-gun, Kyoto 619-0237, Japan

A. M. Vlaicu
National Institute for Material Science, Harima office, SPring-8, Mikazuki, Hyogo 679-5198, Japan

T. Mukoyama
Kanasai Gaidai University, 16-1 Nakamiya-Higashinocho, Hirakata, Osaka 573-1001, Japan
(Received 26 November 2005; published 10 February 2006)

Au $L\beta_2$ satellites were investigated around the L_1 absorption edge with a high-resolution Johann-type spectrometer at the BL15XU undulator beamline SPring-8. The intensities of the $L\beta_2$ satellites were drastically changed at the threshold. Therefore, it is confirmed that the two visible satellites $L\beta_2'$ and $L\beta_2''$ are mainly attributed to the L_1-$L_3M_{4,5}$ Coster-Kronig transitions accompanied by the double-hole states of L_3M_4 or L_3M_5.

DOI: 10.1103/PhysRevA.73.022507 PACS number(s): 32.30.Rj, 32.80.Hd

I. INTRODUCTION

Heavy elements contain a number of electrons that can affect transitions, and the *L-LM* Coster-Kronig (CK) transition reappears in the 5*d* transition elements. Therefore, there is a need for theoretical and experimental investigation of satellites due to such a transition. A number of experiments have examined *L* x-ray satellites of heavy elements. For example, Salgueiro *et al.* and Vlaicu *et al.* [1,2] have examined tungsten and Carvarho *et al.* and us [3,4] have examined gold. However, in these experiments, the elements under examination were excited by electron bombardment or by x rays from an x-ray tube. Therefore, the excitation energy could not be tuned sufficiently. With the advent of the third-generation synchrotron, the threshold behavior of satellites, including the electron correlation, can be examined.

It is well known that the Au $L\beta_2$ diagram line has two satellites $L\beta_2'$ and $L\beta_2''$ on its higher-energy side. Their energy shifts from the diagram line are large enough to confirm their existence in the data. These satellites are therefore called "visible satellites." According to a report by Chen *et al.* [5], the L_1-L_3M_i CK transition is possible for $i=4,5$ in the case of $_{79}$Au. This result agrees with the measured spectra. The $L\beta_2'$ and $L\beta_2''$ satellites have previously been assigned to the L_1M_5-N_5M_5 and L_3M_4-N_5M_4 transitions, respectively. However, the mechanism of the creation of the M_4 or M_5 spectator hole has not been clarified. The M_i spectator hole can be created by either or both the L_3M_i shake process and or the L_1-L_3M_i CK transition. In a previous study, we considered that $L\beta_2'$ and $L\beta_2''$ originated in the $L_3M_{4,5}$ double-hole states created primarily by the L_1-$L_3M_{4,5}$ CK transition. In the present study, the $L\beta_2$ visible satellites are investigated by the evolution of the photoexcited $L\beta_2$ emission spectra in order to elucidate the mechanism of the origin of the satellites.

*Electronic address: hirof@elec.kuicr.kyoto-u.ac.jp

II. EXPERIMENT

Measurements were carried out at BL15XU, SPring-8, Ako, using a curved-crystal x-ray spectrometer [6]. A Si double-crystal monochromator with a bandpass of ~ 3 eV and a flux of $\sim 5\times 10^{11}$ photons/sec was used to generate a tuned x-ray excitation source. BL15XU is a planer-type undulator. Therefore, reducing the harmonic components with the slit is easy. The sample was a 30-μm-thick high-purity Au foil. The fluorescence spectrometer employed Johann geometry with a 1.5-m-diam Rowland circle on a horizontal plane, and Si(100), Si(110), and Si(111) curved crystals can be used to resolve the fluorescence spectra. The spectrometer has a scanning range of 67°–95°. The coherent radiation from the monochromator is radiated onto the sample in the sample chamber of the spectrometer. The fluorescence x-ray beam then passes into the crystal housing, in which three kinds of crystals are mounted. The optical focusing condition can be achieved by moving the sample, crystal, and detector to satisfy Rowland geometry. The spectrometer was evacuated to $\sim 10^{-3}$ torr using a scroll pump. The analyzed fluorescence x-ray spectra were examined using a NaI scintillation counter (SC) or a photon-counting position-sensitive charge-coupled device (CCD). A N_2-gas-filled 7-cm-thick ionization chamber was used to monitor the incident x-ray intensity in front of the sample chamber.

The absorption spectra around the Au L_1 edge and the Au emission spectra of the energy range sufficient to involve $L\beta_2$ and its satellites were measured in advance. Two types of scan were used to investigate the excitation energy dependence of Au $L\beta_2$ satellites. First, the spectrometer was fixed in the Au $L\beta_2''$ peak position and incident x-ray energy was scanned around the Au L_1 edge. An SC with a 0.6-mm slit was attached as the detector, and Si(444) crystal was used in order to obtain high-energy resolution. These conditions provided $\sim$1-eV resolution, referred to herein as the energy-scan mode. Second, Au $L\beta_2$ and $L\beta_2$ satellite emission spec-

TABLE I. Probability of total or partial shake processes at L shell ionization for Au.

	Initial vacancy		
	L_1	L_2	L_3
Total	1.827×10^{-1}	1.847×10^{-1}	1.834×10^{-1}
$\sum_{N,O,P} P_{i,X}$	1.809×10^{-1}	1.825×10^{-1}	1.814×10^{-1}
$\sum_{O,P} P_{i,X}$	1.517×10^{-1}	1.532×10^{-1}	1.522×10^{-1}

tra were measured at excitation energy intervals of 4 eV from 14 350 eV to 14 370 eV, except at 14 366 eV, and at several energy points above and below the Au L_1 edge. The detector was changed to a CCD having a spatial resolution of 20 μm. The spectrometer angle was fixed so as to allow observation of the Au $L\beta_2'$ and Au $L\beta_2''$ without moving the CCD. Si(440) crystal was used in order to measure a wide energy range simultaneously. These conditions provided <1-eV resolution and are referred to herein as evolution mode.

III. DATA ANALYSIS

The instrumental function of the Johann spectrometer is significantly narrower than the widths of Au L emission lines. Therefore, each emission line can be fit well to the Lorentzian. However, the diagram lines include satellite lines. These satellite lines arise from the presence of a spectator hole in the N shell or outer shell and cannot be resolved from the diagram lines because their energy shifts are smaller than the natural widths of the emission lines. These satellite lines are referred to as "hidden satellites" [7]. As in the case of Au $L\beta_2$, the $L\beta_3$ line appeared at a slightly higher energy than that of the $L\beta_2$ line, making separation of the hidden satellites from the $L\beta_2$ line very difficult. Therefore, we used multiplet Lorentzians in the fitting analyses. Mea-

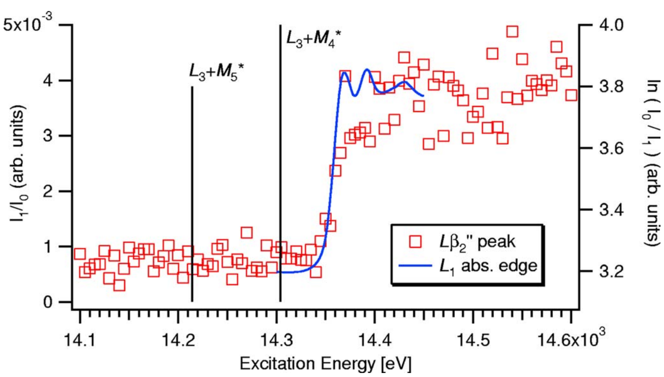

FIG. 1. (Color online) Dependence of $L\beta_2''$ peak height on excitation energy.

TABLE II. Probability of shake processes of each shell at L_3 initial vacancy ionization for Au.

Shell	Total[a]	Shake-up[b]
M_1	1.106×10^{-4}	1.562×10^{-6}
M_2	1.583×10^{-4}	2.200×10^{-6}
M_3	3.798×10^{-4}	4.524×10^{-6}
M_4	5.190×10^{-4}	2.501×10^{-6}
M_5	7.670×10^{-4}	3.966×10^{-6}
N_1	4.046×10^{-4}	1.920×10^{-5}
N_2	6.117×10^{-4}	3.003×10^{-5}
N_3	1.333×10^{-3}	6.283×10^{-5}
N_4	2.586×10^{-3}	5.589×10^{-5}
N_5	3.773×10^{-3}	9.709×10^{-5}
N_6	8.861×10^{-3}	1.622×10^{-5}
N_7	1.166×10^{-2}	1.224×10^{-5}
O_1	1.809×10^{-3}	4.998×10^{-4}
O_2	3.285×10^{-3}	1.072×10^{-3}
O_3	7.673×10^{-3}	2.666×10^{-3}
O_4	3.948×10^{-2}	1.926×10^{-2}
O_5	7.038×10^{-2}	3.923×10^{-2}
P_1	2.959×10^{-2}	2.738×10^{-2}

[a]All shake-up and shake-off.
[b]All shake-up.

sured spectra of the $L\beta_{2,15,3}$, L_3M_5-M_5N_5, and L_3M_4-M_4N_5 satellites were analyzed using five Lorentzians. Because the $L\beta_2$ lines include hidden satellites, Lorentzians were used for $L\beta_2$ to describe the multiplet of the diagram line and many hidden satellites—namely, L_3X-$XN_5(X=N_1,N_2,\ldots,N_7)$ [2,8]. Other satellites caused by a spectator hole in the O shell or P shell were not included in the multiplet. Because they have approximately the same energy as the diagram line, their influence on the width and asymmetry of the diagram line can be neglected.

Multiconfiguration Dirac-Fock (MCDF) calculations based on the average level (AL) version of the GRASP2 code [9] were performed in order to find the number and energy shift of satellites for each spectator hole. All hidden satellites were assumed to have the same width as that of the diagram line.

The relative intensities of the satellite lines were calculated assuming that the fluorescence yields and the fractical emission rates are the same for both single-vacancy states and multiple-vacancy states. This is not strictly correct, but rather it is a crude estimation to describe quantitatively the simplest model of deexcitation.

The satellite lines are believed to be the radiative decay of double-vacancy states due to either the CK transition or the shake process. Multiple CK transitions and a combination of the CK transition and the shake process can also occur within the ionization process. However, the combined processes can be ignored due to the low probabilities. When satellite lines are caused by a single CK transition, the intensity of the diagram line $L\beta_2$ can be calculated as

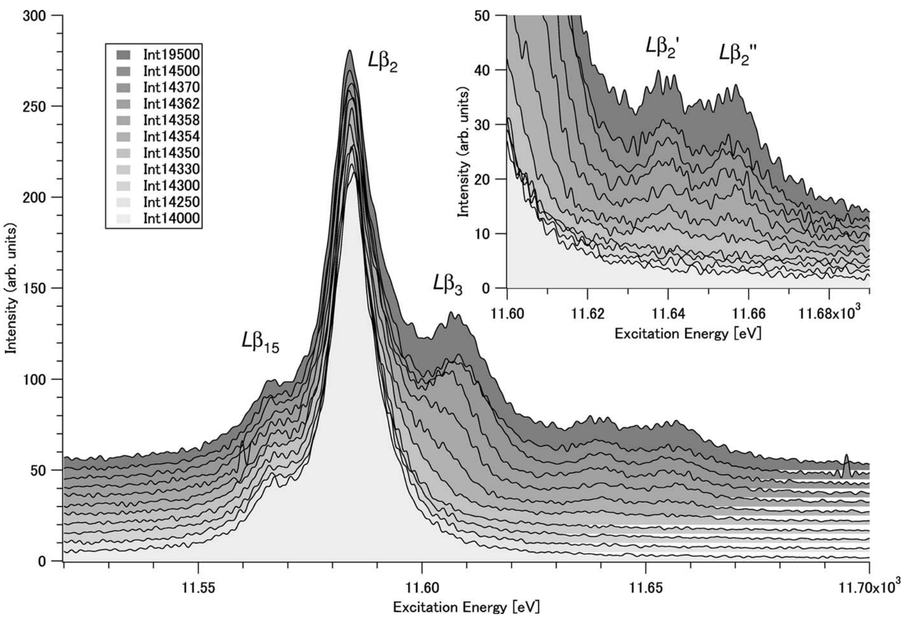

FIG. 2. Change in Au $L\beta_2$, $L\beta_3$, $L\beta_{15}$, and $L\beta_2$ visible satellite spectra near the Au L_1 edge.

$$I_M(L\beta_2) = C\sigma_3(1-P_3)\omega_3\frac{\Gamma(L\beta_2)}{\Gamma_3}, \quad (1)$$

where C is a constant, $\sigma_i(i=1,2,3)$ are ionization cross sections by photons of the L_i subshell, P_i is the probability of all possible shake processes accompanied by L_i ionization, ω_i is the fluorescence yield for the L_i subshell, and $\Gamma(L\beta_2)/\Gamma_3$ is the fractical emission rate for the $L\beta_2$ line from the L_3 subshell.

For $L\beta_2$ satellite lines, the transition to the initial vacancy state L_3 can occur by two possible CK transitions: L_1-L_3X and L_2-L_3X. In addition, L_3X double-hole states can also be created when the shake process occurs during the ionization of L_3. The intensity of each spectator hole satellite line consists of three terms:

$$I_S(L\beta_2) = C\sigma_1(1-P_1)f_{1,3}p(L_1L_3X)\omega_3\frac{\Gamma(L\beta_2)}{\Gamma_3} + C\sigma_2(1-P_2) \times f_{2,3}p(L_2L_3X)\omega_3\frac{\Gamma(L\beta_2)}{\Gamma_3} + C\sigma_3P_{3,X}\omega_3\frac{\Gamma(L\beta_2)}{\Gamma_3}, \quad (2)$$

where $f_{i,j}$ is the partial CK transition probability from level L_i to level L_j, $p(L_iL_jX)$ is the probability of the radiationless transition L_i-L_jX that results in the double-vacancy state L_jX, and $P_{i,X}$ is the probability of all possible shake processes from the X orbital accompanied by L_i ionization. Values reported by Campbell were used for ω_i and $f_{i,j}$ [10]. For σ_i, values interpolated from the report by Scofield [11] and our measured data were used. For $p(L_iL_jX)$, the values of $_{80}$Hg reported by Chen *et al.* [12] were used. Values related to the shake process were calculated relativistically using the Dirac-Fock-Slater wave functions in sudden approximation [13]. These values are shown in Tables I and II. In these equations, $\Sigma_{N,O,P}P_{i,X}$ are used as P_3 and P_2, and $\Sigma_{O,P}P_{1,X}$ is used as P_1, at the excitation energy around the L_1 edge (from 14 000 eV to 14 500 eV). Total probability is used for P_i at sufficiently high energy (19 500 eV).

The relative intensities of hidden satellites to the diagram line were acquired from Eqs. (1) and (2) in the case of $X=N_1,N_2,\ldots,N_7$. The intensities of satellites for $X=O,P$ are included in that of the diagram line. The energy shifts and relative intensities of hidden satellites in the fitting were fixed.

IV. RESULTS AND DISCUSSION

A. Energy scan

It is generally considered that the double-hole state L_3M_4, which is the initial state of $L\beta_2''$, is ascribed to two processes. One process is the L_3M_4 shake process. This is the excitation process, so that its transition probability depends directly on the excitation energy. The onset of this process can be estimated to be $L_3+M_4^*$ binding energies (* denotes the $Z+1$ element; $_{79}$Au M_4^* means $_{80}$Hg M_4). The other process is the L_1-L_3M_4 CK transition process. This is the relaxation process and is therefore independent of the excitation energy. The data of the energy-scan mode measurement are shown in Fig. 1. The measured $L\beta_2''$ intensity is normalized by the incident x-ray beam intensity. The L_1 absorption spectra and $L_3+M_4^*/M_5^*$ are also shown in Fig. 1 as energy references. This method is equivalent to x-ray-absorption fine-structure (XAFS) spectroscopy using the $L\beta_2''$ partial fluorescence yield (PFY). The threshold of the appearance of $L\beta_2''$ appears to be that of the L_1 edge rather than that of $L_3+M_4^*$. The intensity of $L\beta_2''$ shows almost the same tendency as the L_1-edge-absorption spectra, increasing suddenly at the L_1 edge and becoming approximately constant above the L_1 edge. This suggests that $L\beta_2''$ is ascribed to the L_1 vacancy. However, this requires measurement of the $L\beta_{2,3,15}$ emission spectra in order to confirm the effect of $L\beta_3(L_1$-$M_3)$.

B. Evolution

The evolution of the $L\beta_{2,3,15}$ emission spectra around the L_1 edge are shown in Fig. 2.

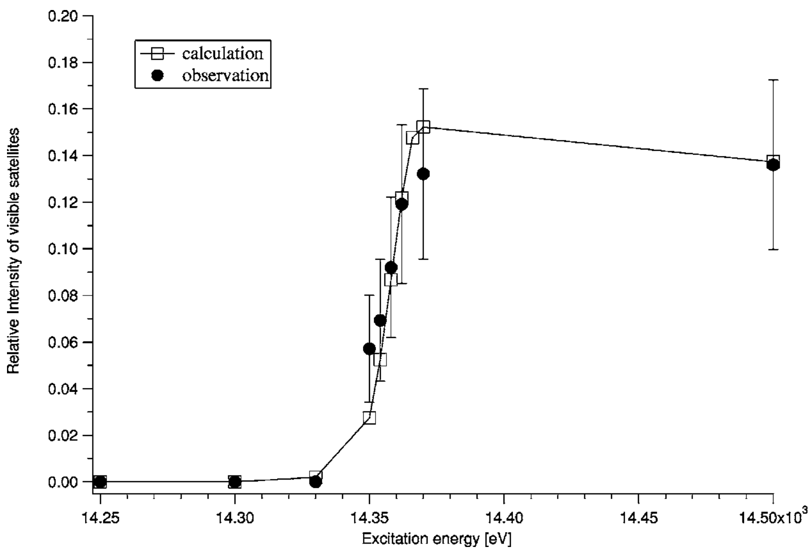

FIG. 3. Excitation energy dependence of the relative intensity of the sum of Au $L\beta_2$ visible satellites on the $L\beta_2$ diagram line.

Previously, these spectra were studied only for high-energy excitation in conventional x-ray tubes [14–16]. The most outstanding feature of the data is the abrupt increase in the satellite intensity over a considerable energy range around the threshold. Figure 2 indicates that the $L\beta_3$ diagram line and both $L\beta_2$ visible satellites appear around the L_1 edge with the excitation energy.

The spectra obtained by the CCD camera were analyzed by fitting the $L\beta_{2,3,15}$ diagrams and $L\beta_2$ satellites by the multiplet Lorentzian profile (see Sec. III). We obtained the relative intensities of satellites to the diagram line. According to the results of MCDF calculations, the M satellites, which consist of several multiplets, have wide widths and partly overlap each other. Therefore, we took the sum of $L\beta_2'$ and $L\beta_2''$ as the intensity of the visible satellites.

Because the L_2-L_3M CK transition is energetically forbidden in the case of Au, Eq. (2) for visible satellites becomes as follows:

$$I_{VS}(L\beta_2) = C\sigma_1(1 - P_1)f_{1,3}p(L_1L_3M)\omega_3\frac{\Gamma(L\beta_2)}{\Gamma_3} + C\sigma_3P_{3,M}\omega_3\frac{\Gamma(L\beta_2)}{\Gamma_3}. \tag{3}$$

The relative intensity of the visible satellites to the diagram-line-related hidden satellites can be calculated from Eqs. (1)–(3) at each excitation energy.

The dependence of the relative intensity of visible satellites to the diagram line on the excitation energy both by calculation and by observation is shown in Fig. 3. The relative intensities of visible satellites to the diagram line $L\beta_2$ increase along with the L_1-absorption spectra. This behavior is similar to the abrupt edgelike behavior. In the range of excitation energy above the L_1 edge, these intensities are approximately constant. The calculated data plots agree very well with the observed data.

The relative intensity of the sum of $L\beta_2$ visible satellites to the $L\beta_2$ diagram line depends on the shake-off probability P and the ratio of photoionization cross sections of the L_1 and L_3, σ_1/σ_3, from Eqs. (1) and (3). $P_{3,M}$ is composed almost entirely by shake-off and hardly changes in the narrow range around the L_1 edge (Table II), and the increase in the relative intensity of visible satellites is ascribed to the increase of σ_1/σ_3, which indicates that the L_1-L_3M CK transition is dominant for the origin of $L\beta_2$ visible satellites.

When the diagram line is excited at an energy near the threshold of its appearance, a Raman shift to that line occurs. In this measurement, the Raman shift of $L\beta_3$ can be seen in the energy range across the L_1 edge (see Fig. 2). However, the Raman shift is not seen in the $L\beta_2$ visible satellites around the L_1 edge, which is the threshold of their appearance. This also indicates that the radiative transitions of the visible satellites are not related to the L_1 subshell.

V. CONCLUSIONS

In the present study, we have examined the near threshold of the $L\beta_2$ satellites ascribed to the CK transition in Au. The observed $L\beta$ spectra are analyzed by a single Lorentzian fitting. The energy dependence of the ratio of the $L\beta_2$ visible satellites to the diagram line shows a tendency that is similar to that of the L_1-absorption spectra.

The contribution of the CK transition to Au $L\beta$ satellites was clearly confirmed. That is, Au $L\beta_2$ visible satellites are caused primarily by the L_1-L_3M_i $(i=4,5)$ CK transition. Further investigations are planned in order to elucidate the details of the dependence of the intensity in the satellites on the excitation energy in heavy elements.

ACKNOWLEDGMENTS

The present study was performed under proposal Nos. C03A15XU-2004N and C05A15XU-2001N, and under the guidance of the Kyoto Prefecture Collaboration of Regional Entities for the Advancement of Technological Excellence, JST.

[1] L. Salgueiro, M. L. Carvalho, and F. Parente, J. Phys. (Paris), Colloq. **48**, C9-609 (1987).

[2] A. M. Vlaicu, T. Tochio, T. Ishizuka, D. Ohsawa, Y. Ito, T. Mukoyama, A. Nisawa, T. Shoji, and S. Yoshikado, Phys. Rev. A **58**, 3544 (1998).

[3] M. L. Carvalho, F. Parente, and L. Salgueiro, J. Phys. B **20**, 935 (1987).

[4] H. Oohashi, T. Tochio, Y. Ito, and A. M. Vlaicu, Phys. Rev. A **68**, 032506 (2003).

[5] M. H. Chen, B. Crasemann, K.-N. Huang, M. Aoyagi, and H. Mark, At. Data Nucl. Data Tables **19**, 97 (1977).

[6] N. Shigeoka, H. Oohashi, Y. Ito, A. M. Vlaicu, A. Nisawa, and H. Yoshikawa, in *Application of Accelerators in Research and Industry*, edited by J. L. Duggan and I. L. Morgan, AIP Conf. Proc. No. 680 (AIP, Melville, NY, 2003), pp. 20–23.

[7] B. K. Agarwal, *X-ray Spectroscopy* (Springer-Verlag, New York, 1979).

[8] M. Deutsch, G. Hölzer, J. Härtwig, J. Wolf, M. Fritsch, and E. Förster, Phys. Rev. A **51**, 283 (1995).

[9] I. P. Grant, B. J. McKenzie, P. H. Norrington, D. F. Mayers, and N. C. Pyper, Comput. Phys. Commun. **21**, 207 (1980).

[10] J. L. Campbell, At. Data Nucl. Data Tables **85**, 291 (2003).

[11] J. H. Scofield, Lawrence Livermore Radiation Laboratory Report No. UCRL-51326, 1973 (unpublished).

[12] M. H. Chen, B. Craseman, and H. Mark, At. Data Nucl. Data Tables **24**, 13 (1979).

[13] T. Mukoyama, Y. Ito, and K. Taniguchi, X-Ray Spectrom. **28**, 491 (1999).

[14] J. H. William, Phys. Rev. **45**, 71 (1934).

[15] F. K. Richtmyer, S. W. Barnes, and E. Ramberg, Phys. Rev. **46**, 843 (1934).

[16] P. Amorim, L. Salgueiro, F. Parente, and J. G. Ferreira, J. Phys. B **21**, 3851 (1988).